

Synchronous optical pumping of quantum revival beats for atomic magnetometry

S. J. Seltzer, P. J. Meares, and M. V. Romalis

Department of Physics, Princeton University, Princeton, New Jersey 08544, USA

(Received 16 May 2006; published 30 May 2007)

We observe quantum beats with periodic revivals due to nonlinear spacing of Zeeman levels in the ground state of potassium atoms, and demonstrate their synchronous optical pumping by double modulation of the pumping light at the Larmor frequency and the revival frequency. We show that synchronous pumping increases the degree of spin polarization by a factor of 4. As a practical example, we explore the application of this double-modulation technique to atomic magnetometers operating in the geomagnetic field range, and find that it can increase the sensitivity and reduce magnetic-field-orientation-dependent measurement errors endemic to alkali-metal magnetometers.

DOI: [10.1103/PhysRevA.75.051407](https://doi.org/10.1103/PhysRevA.75.051407)

PACS number(s): 32.80.Bx, 07.55.Ge, 32.30.Dx, 42.50.Md

Periodic revival of quantum beats is a general phenomenon that occurs in multilevel systems with nonlinear energy level spacing [1,2] and has been observed in diverse systems, from one-atom masers [3] and Rydberg states in atoms [4] to molecular vibrational [5] and rotational [6] states. Recently, molecular rotational revivals attracted significant attention because of the possibility of using them for alignment of molecules with ultrashort laser pulses [7–10]. It has been proposed that periodic laser pulses could be used to increase the degree of molecular alignment and maintain it indefinitely [11–14]. An increase of molecular alignment using two pulses has been demonstrated in [9].

Here we show experimentally that an appropriately synchronized train of laser pulses can increase the degree of spin orientation and maintain it indefinitely by synchronously pumping quantum revivals in the ground-state Zeeman levels of an alkali-metal atom. Periodic revivals of quantum beats in Zeeman levels of alkali-metal atoms occur naturally due to nonlinear Breit-Rabi mixing [15] and have been modeled in [16]. We observe quantum revivals in K atoms and demonstrate their synchronous pumping by double modulation of the pump laser at both the Larmor and the revival frequencies. We find that this creates a coherently oscillating superposition state with a spin polarization a factor of 4 higher than can be obtained without double modulation for the same average laser power. We also model the effects in other alkali-metal atoms and find that the amount of polarization enhancement increases for systems with a larger number of quantum states.

Because the revivals occur in the geomagnetic field range of about 0.5 G, our experiments are also directly applicable to optically pumped alkali-metal magnetometers, which are used in many applications, from archaeology [17] and mineral exploration [18] to searches for a *CP*-violating electric dipole moment [19]. As was recently discussed in [20,21], Breit-Rabi mixing of Zeeman levels decreases magnetometer sensitivity by splitting the Zeeman resonance into many separate lines. We show that synchronous pumping of quantum revivals largely recovers the signal loss. In addition, we demonstrate that it generates a symmetric resonance line shape, reducing a systematic effect endemic to most alkali-metal magnetometers, known as a heading error, that causes changes in the measured absolute value of the magnetic field depending on the orientation of the magnetometer with re-

spect to the magnetic field vector [22]. We expect that synchronous pumping of revivals can also be used to improve the precision and accuracy of spectroscopic measurements on other multilevel systems.

For alkali-metal atoms with nuclear spin I , the energy levels of the two hyperfine states with $F=I\pm 1/2$ in a magnetic field B are given by the well-known Breit-Rabi equation [15]. Following the general description of quantum revivals in multilevel systems [2], the energy levels can be expanded in powers of m_F , keeping only the leading B dependence in each term,

$$E(F, m_F) = -\frac{h\nu_{\text{hf}}}{2(2I+1)} + (-g_I\mu_N \pm \mu_{\text{eff}})Bm_F \mp \frac{\mu_{\text{eff}}^2 B^2 m_F^2}{h\nu_{\text{hf}}} \pm 2\frac{\mu_{\text{eff}}^3 B^3 m_F^3}{(h\nu_{\text{hf}})^2}, \quad (1)$$

where $\mu_{\text{eff}} = (g_s\mu_B + g_I\mu_N)/(2I+1)$, $h\nu_{\text{hf}}$ is the hyperfine splitting of the ground state, $g_I = \mu_I/(\mu_N I)$ is the nuclear g factor, μ_I is the nuclear magnetic moment, $g_s \approx 2$ is the electronic g factor, μ_N is the nuclear magneton, and μ_B is the Bohr magneton. The Larmor frequency corresponds to classical spin precession $\nu_L = (-g_I\mu_N \pm \mu_{\text{eff}})B/h$, the revival frequency is given by $\nu_{\text{rev}} = \mu_{\text{eff}}^2 B^2/h^2 \nu_{\text{hf}}$, and the super-revival frequency is $\nu_{\text{suprev}} = 2\mu_{\text{eff}}^3 B^3/h^3 \nu_{\text{hf}}^2$. For ^{39}K atoms ($I=3/2$, $g_I=0.26$, $\nu_{\text{hf}}=461.7$ MHz) in a magnetic field $B=0.5$ G we have $\nu_L=350$ kHz, $\nu_{\text{rev}}=265$ Hz, and $\nu_{\text{suprev}}=0.4$ Hz.

The experiments are performed in a 5-cm-diameter evacuated spherical Pyrex cell with a 1-mm-diameter, 5-cm-long stem containing K metal in natural abundance (93% ^{39}K and 7% ^{41}K). The cell is heated to 60 °C by hot air in a double-walled glass oven. The cell walls are coated with octadecyltrichlorosilane (OTS) to reduce surface spin relaxation of K atoms. OTS molecules [$\text{CH}_3-(\text{CH}_2)_{17}-\text{Si}-\text{Cl}_3$] attach to glass through a silanization reaction, and ideally expose alkali-metal atoms only to a surface of long hydrocarbon chains, known to reduce wall relaxation due to their low polarizability [23]. We have used the coating procedure described in [24] and obtained a K longitudinal spin relaxation time T_1 up to 145 ms, corresponding to 2100 collisions with the walls before depolarization, although the relaxation times were not entirely consistent and other cells coated in the same batch

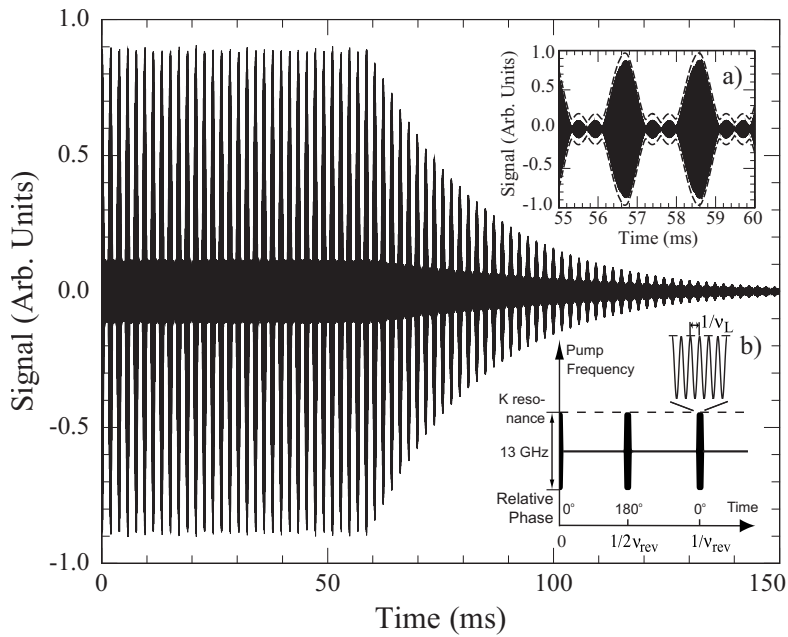


FIG. 1. Measurement of $\langle S_x \rangle$ showing multiple quantum revivals. Synchronous pumping of quantum revivals is started 150 ms before $t=0$ and stopped at $t=60$ ms, allowing free decay of spin coherence. Inset (a) shows a comparison of the revival envelope with a density matrix simulation (dashed lines slightly offset vertically for visibility), while inset (b) shows double modulation of the pump laser frequency, so the optical pumping occurs only during instances of maximum expectation value of $\langle S_z \rangle$.

had T_1 of 1.6, 20, and 61 ms. The longitudinal spin relaxation time did not degrade and actually improved in some cells when they were heated to 120 °C for a period of weeks. In magnetic resonance measurements we found that T_2 was limited by relaxation due to magnetic field gradients to about 30 ms.

In most measurements we use the Bell-Bloom technique [25] of spin resonance excitation using a pump laser modulated at the Larmor frequency. The cell is placed in three orthogonal Helmholtz coils which are used to control the magnitude and direction of the magnetic field, as well as five gradient coils used to cancel ambient field gradients. The field is nominally set along the \hat{y} direction, and magnetic field noise along this direction is actively canceled using feedback from a fluxgate sensor (Bartington Instruments Mag-03MC) located next to the oven. The atoms are pumped by circularly polarized light from a distribution feedback diode laser propagating along the \hat{z} direction. The laser is detuned by approximately 6.3 GHz off the potassium $D1$ resonance at 770.1 nm, much larger than the measured 0.9 GHz Doppler-broadened half-width of the optical line. The laser current is sinusoidally modulated at the Larmor frequency so that the laser frequency reaches the resonance only for a short fraction of each cycle. For synchronous pumping of quantum revivals, a secondary modulation is applied at twice the revival frequency, turning the Larmor frequency current modulation on and off with a duty cycle in the range of 1–10%, as shown in Fig. 1(b). In addition, the relative phase of the Larmor modulation is changed by 180° for odd modulation pulses. In frequency space, this creates sidebands of the optical pumping rate that are located at $\nu_L \pm \nu_{\text{rev}}(2n+1)$, $n=0, 1, 2, \dots$. When the high-frequency modulation is tuned exactly to ν_L for $F=2$, the sidebands of the pumping rate modulation simultaneously excite all $F=2$ Zeeman transitions. Simultaneous excitation of two Zeeman coherences in an atomic magnetometer has been previously demonstrated in [26]. The pump beam power is always adjusted to broaden

the magnetic resonance width by a factor of 2, which gives the same average pumping rate that approximately maximizes the signal-to-noise ratio in atomic magnetometers.

The $\langle S_x \rangle$ component of spin polarization is probed using optical rotation of a DFB laser beam propagating along the \hat{x} direction and detuned about 1 GHz away from the $D1$ resonance. Synchronous optical pumping of quantum revivals is shown in Fig. 1 with a 10% duty cycle for secondary modulation. Beating between different Zeeman coherences causes the polarization envelope to reappear with a period $1/\nu_{\text{rev}}$. As shown in Fig. 1(a), the shape of the revival envelope is in agreement with a density matrix simulation. The revivals persist indefinitely, until at $t=60$ ms the pumping light is turned off, showing free spin precession with many quantum revivals with amplitude decaying due to spin relaxation.

To obtain a magnetic resonance signal, the amplitude of optical rotation at the Larmor frequency, proportional to $\langle S_x \rangle$, is recorded by a lock-in amplifier and sampled by a sample-and-hold circuit triggered at times of maximum revival. For optimal detection of spin precession, the probe laser can be turned on only during revivals with a duty factor d and power increased by a factor of $1/d$ relative to optimal continuous measurement, giving the same shot-noise sensitivity.

Figure 2 shows the magnetic resonance spectrum for $B \approx 0.5$ G as a function of Larmor modulation frequency of the pump laser current both with (dashed lines) and without (solid lines) secondary modulation at 530 Hz with a 1% duty cycle. Without secondary modulation the resonance spectrum consists of four lines corresponding to individual $F=2$, $m_F \rightarrow m_F+1$ Zeeman transitions. With secondary modulation there is a central resonance at ν_L , strictly proportional to the magnetic field, and a number of sidebands spaced by $2\nu_{\text{rev}}$. The density matrix simulation shown in Fig. 2(a) predicts that the maximum spin polarization is increased by a factor of 6 relative to the case without secondary modulation, due to constructive interference between all Zeeman coherences; the experimental data plotted in Fig. 2(b) show an increase of

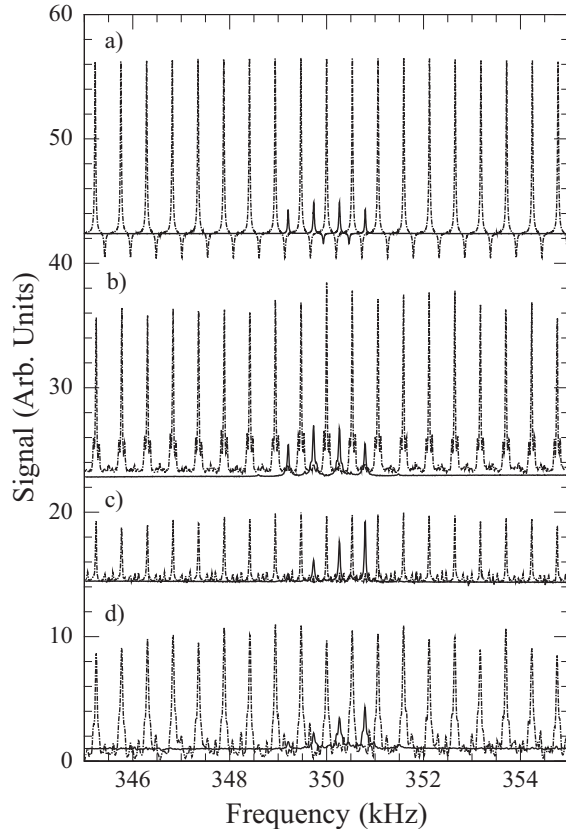


FIG. 2. Magnetic resonance spectra in a 0.5 G field with (dashed lines) and without (solid lines) secondary modulation at twice the revival frequency. Numerical simulation (a) and experimental measurements with magnetic field in \hat{y} direction (b) and tilted by 60° into the \hat{z} direction (c) with optical excitation of spin precession. (d) “ M_x ” magnetometer signal with rf excitation and magnetic field in \hat{z} direction. The signals are offset in the vertical direction by an arbitrary amount. Small random variations in the height of the peaks with secondary modulation and small sidebands are due to 60 Hz noise.

the spin polarization by a factor of 3.9. The linewidth of the resonances is kept the same, so higher spin polarization directly translates into higher magnetometer sensitivity.

The heading errors in atomic magnetometers can be simply understood as resulting from overlap of the multiple Zeeman resonances [22]. For well-resolved resonances, as in Fig. 2, the magnetometer is locked to the strongest resonance and the heading error is due to tails of other resonances that change in size depending on the orientation of the pump laser relative to the magnetic field because of changes in the longitudinal spin polarization. The frequency shift of a particular resonance with frequency ν_0 and amplitude A_0 due to the tails of other Lorentzian resonances can be estimated as

$$\Delta\nu = \frac{\Gamma^2}{A_0} \sum_i \frac{A_i}{\nu_i - \nu_0}, \quad (2)$$

where Γ is the half width at half maximum, assumed to be the same for all resonances, and ν_i and A_i are the frequencies and relative heights of the other resonance lines. Magneto-

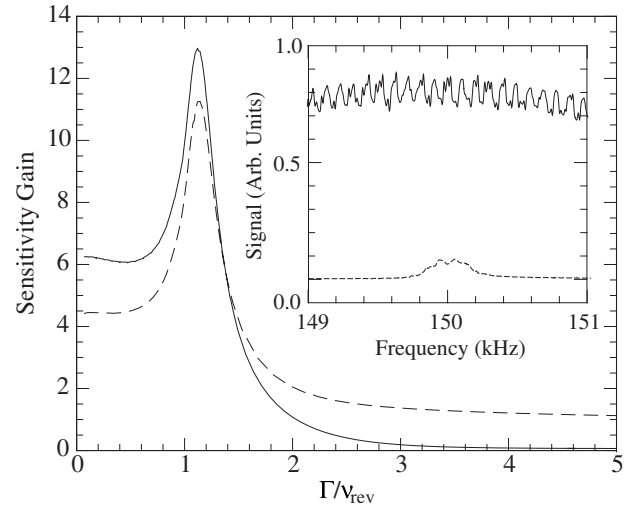


FIG. 3. Calculated gain in magnetometer sensitivity due to higher spin polarization for secondary modulation with 1% (solid line) and 30% (dashed line) duty cycle relative to the case with no secondary modulation. The average optical pumping rate is set equal to the relaxation rate. The inset shows experimental magnetic resonance spectrum in a 0.21 G field with increased magnetic field gradients. Secondary modulation (solid line) shows individual resonances which are poorly resolved without it (dashed line).

meter signals recorded with the magnetic field tilted by 60° from the y axis in the direction of the pump laser are shown in Fig. 2(c). The relative strengths of Zeeman resonances without secondary modulation change significantly, depending on field orientation, leading to a heading error given by Eq. (2). In contrast, the resonance lines obtained with secondary modulation are symmetrical and do not systematically change relative size with tilting of the field, so the tails of various peaks cancel and do not lead to a significant heading error.

We also point out the general applicability of the double-modulation technique by demonstrating that it works for a common “ M_x ”-type magnetometer [22] using a rf field to excite spin precession. For these measurements the magnetic field is directed along \hat{z} , parallel to the pump laser, which is not modulated and remains tuned to the $D1$ resonance. Spin precession is excited by a transverse rf field at the Larmor frequency, which is similarly modulated at twice the revival frequency with 1% duty cycle and 180° phase reversal for odd pulses. The solid line in Fig. 2(d) shows continuous rf excitation while the dashed line shows rf excitation with secondary modulation. The amplitude of the rf field is adjusted to generate the same level of rf broadening, ensuring equal widths of the resonances. As with optical excitation, we observe an increase in sensitivity by approximately a factor of 3 and a symmetrical set of sidebands that does not cause a significant heading error.

We use a numerical simulation for a general analysis of polarization gains and heading errors. We calculate the time evolution of the alkali-metal ground-state density matrix in the presence of doubly modulated pumping and simulate lock-in detection, generating resonance spectra [see Fig. 2(a)] that are similar to experimental data. The magneto-

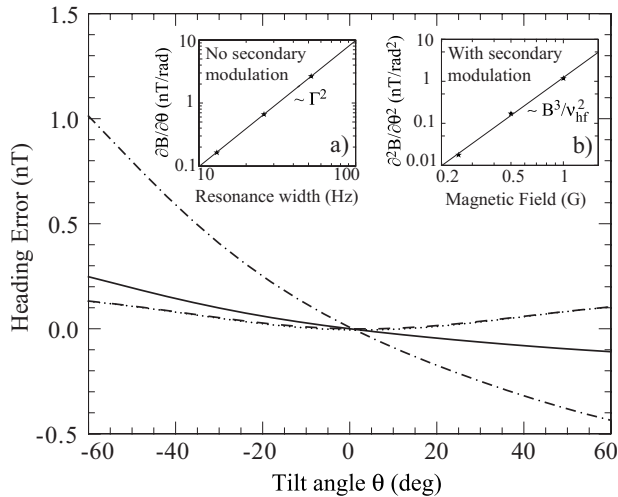


FIG. 4. Heading error determined from numerical simulation as a function of the magnetic field tilt angle θ away from the y axis into the direction of the pump beam. With no secondary modulation the heading error depends on the resonance linewidth (solid line, $\Gamma=13$ Hz; dash-dotted line, $\Gamma=26$ Hz), while with secondary modulation the heading error is approximately quadratic in θ and is independent of the resonance linewidth (dashed line, $\Gamma=13$ Hz; dotted line, $\Gamma=26$ Hz). Inset (a) shows that without secondary modulation the slope of the heading error near $\theta=0$ scales as Γ^2 . Inset (b) shows that with secondary modulation the curvature of the heading error near $\theta=0$ scales as B^3 , indicating that it is due to third-order splitting of the energy levels.

ter sensitivity and the resonance frequency are determined, respectively, from the slope and the zero crossing of the dispersion curves. Figure 3 shows the gain in sensitivity due to higher spin polarization for K as a function of resonance linewidth. We also investigated the case of Cs with $I=7/2$, and found that the increase in maximum spin polarization and the gain in sensitivity are about a factor of 2 higher than

in K, due to coherent interference of a larger number of levels. Secondary modulation also helps to resolve individual resonances when $\Gamma \sim \nu_{\text{rev}}$, as demonstrated experimentally in the inset of Fig. 3, leading to additional gain in sensitivity over the case of continuous pumping in this regime. The heading error, which is usually on the order of ν_{rev} when the individual resonances are poorly resolved, can also be significantly reduced by locking to one of the resolved resonances, which remain symmetrical when the magnetic field is tilted.

In Fig. 4 we show the heading error as a function of magnetic field tilt angle θ into the direction of the pump beam. Without secondary modulation the heading error is approximately linear near $\theta=0$ and scales with the square of the resonance linewidth Γ , as predicted by Eq. (2). In contrast, the heading error with secondary modulation is quadratic near $\theta=0$ and does not depend on the resonance linewidth, making the magnetometer less susceptible to magnetic gradient broadening; it is instead due to cubic energy level splitting and scales as B^3/ν_{hf}^2 . We expect the heading error with secondary modulation to be much smaller for Rb or Cs with larger ν_{hf} . For comparison, most existing atomic magnetometers have heading errors on the order of 10 nT and can achieve the 0.1 nT level only with very narrow resonance lines [22].

In conclusion, we have demonstrated synchronous pumping of quantum revivals and shown that it can be used to increase the degree of atomic orientation. We also find that the resulting resonance line shape is symmetric, which is important for reducing systematic errors in frequency measurements on multilevel systems. Our results are directly applicable to alkali-metal magnetometers operating in the geomagnetic field range and can be used to increase their sensitivity and reduce heading errors.

This work was funded by an Office of Naval Research MURI grant and the NSF.

-
- [1] C. Leichtle, I. S. Averbukh, and W. P. Schleich, Phys. Rev. Lett. **77**, 3999 (1996).
 [2] R. W. Robinett, Phys. Rep. **392**, 1 (2004).
 [3] G. Rempe, H. Walther, and N. Klein, Phys. Rev. Lett. **58**, 353 (1987).
 [4] J. A. Yeazell, M. Mallalieu, and C. R. Stroud, Jr., Phys. Rev. Lett. **64**, 2007 (1990).
 [5] R. M. Bowman, M. Dantus, and A. H. Zewail, Chem. Phys. Lett. **161**, 297 (1989).
 [6] F. Rosca-Pruna and M. J. J. Vrakking, Phys. Rev. Lett. **87**, 153902 (2001).
 [7] T. Seideman, Phys. Rev. Lett. **83**, 4971 (1999).
 [8] H. Stapelfeldt and T. Seideman, Rev. Mod. Phys. **75**, 543 (2003).
 [9] C. Z. Bisgaard, M. D. Poulsen, E. Péronne, S. S. Viftrup, and H. Stapelfeldt, Phys. Rev. Lett. **92**, 173004 (2004).
 [10] D. Daems *et al.*, Phys. Rev. Lett. **95**, 063005 (2005).
 [11] M. Leibscher, I. Sh. Averbukh, and H. Rabitz, Phys. Rev. Lett. **90**, 213001 (2003).
 [12] M. Leibscher, I. Sh. Averbukh, and H. Rabitz, Phys. Rev. A **69**, 013402 (2004).
 [13] J. Ortigoso, Phys. Rev. Lett. **93**, 073001 (2004).
 [14] J. Ortigoso and J. Santos, Phys. Rev. A **72**, 053401 (2005).
 [15] G. Breit and I. I. Rabi, Phys. Rev. **38**, 2082 (1931).
 [16] E. B. Alexandrov *et al.*, J. Opt. Soc. Am. B **22**, 7 (2005).
 [17] A. David *et al.*, Antiquity **78**, 341 (2004).
 [18] M. N. Nabighian *et al.*, Geophysics **70**, 33 (2005).
 [19] S. Groeger, A. S. Pazgalev, and A. Weis, Appl. Phys. B: Lasers Opt. **80**, 645 (2005).
 [20] P. D. D. Schwindt, L. Hollberg and J. Kitching, Rev. Sci. Instrum. **76**, 126103 (2005).
 [21] V. Acosta *et al.*, Phys. Rev. A **73**, 053404 (2006).
 [22] E. B. Alexandrov, Phys. Scr., T **105**, 27 (2003).
 [23] M. A. Bouchiat and J. Brossel, Phys. Rev. **147**, 41 (1966).
 [24] M. S. Rosen *et al.*, Rev. Sci. Instrum. **70**, 1546 (1999).
 [25] W. E. Bell and A. L. Bloom, Phys. Rev. Lett. **6**, 280 (1961).
 [26] M. V. Balabas, V. A. Bonch-Bruevich, and S. V. Provotorov, Sov. Tech. Phys. Lett. **15**, 287 (1989).